HHS Public Access

Author manuscript

Cell Stem Cell. Author manuscript; available in PMC 2016 April 08.

Published in final edited form as:

Cell Stem Cell. 2015 October 1; 17(4): 486–498. doi:10.1016/j.stem.2015.07.010.

Circulating IGF-I and IGFBP3 levels control human colonic stem cell function and are disrupted in diabetic enteropathy

Francesca D'Addio[#1,2], **Stefano La Rosa**[#3], **Anna Maestroni**[2], **Peter Jung**[4], **Elena Orsenigo**[5], **Moufida Ben Nasr**[1,2], **Sara Tezza**[1,2], **Roberto Bassi**[1,2], **Giovanna Finzi**[3], **Alessandro Marando**[3], **Andrea Vergani**[1,2], **Roberto Frego**[6], **Luca Albarello**[7], **Annapaola Andolfo**[8], **Roberta Manuguerra**[9], **Edi Viale**[6], **Carlo Staudacher**[5], **Domenico Corradi**[9], **Eduard Batlle**[4,10], **David Breault**[11], **Antonio Secchi**[2,12], **Franco Folli**[13,14], and **Paolo Fiorina**[1,2,*]

[1]Nephrology Division, Boston Children's Hospital, Harvard Medical School, Boston 02115, MA, USA

[2]Transplant Medicine, IRCCS Ospedale San Raffaele, Milan 20132, Italy

[3]Department of Pathology, Ospedale di Circolo, Varese 21100, Italy

[4]Institute for Research in Biomedicine (IRB Barcelona), Barcelona 08028, Spain

[5]Surgery, Protein Microsequencing Facility, IRCCS Ospedale San Raffaele, Milan 20132, Italy

[6]Gastroenterology, Protein Microsequencing Facility, IRCCS Ospedale San Raffaele, Milan 20132, Italy

[7]Pathology Unit, Protein Microsequencing Facility, IRCCS Ospedale San Raffaele, Milan 20132, Italy

[8]ProMiFa, Protein Microsequencing Facility, IRCCS Ospedale San Raffaele, Milan 20132, Italy

[9]Department of Biomedical, Biotechnological and Translational Sciences, Unit of Pathology, University of Parma, Parma 43121, Italy

[10]Institució Catalana de Recerca i Estudis Avançats (ICREA), Barcelona 08028, Spain

[11]Division of Endocrinology, Boston Children's Hospital, Harvard Medical School, Boston 02115, MA, USA

[12]Vita Salute San Raffaele University, Milano 20132, Italy

[13] Department of Medicine, Division of Diabetes, University of Texas Health Science Center at San Antonio, San Antonio 78229, Texas, USA

[*]Corresponding Author. **Paolo Fiorina, MD PhD**, Nephrology Division, Boston Children's Hospital, Harvard Medical School, 300 Longwood Ave. Enders Building 5th floor En511, Boston MA 02115, Tel. +1 617 919 2624, Fax. +1 627 732 5254, paolo.fiorina@childrens.harvard.edu.

Author contributions

F.D. and S.LR. designed the study, performed experiments, analyzed data, and wrote the paper; A. Maestroni, E.O., M.BN., S.T., R.B. and A.V. performed experiments and analyzed data; G.F. and A. Marando helped with histology and electron microscopy analysis; R.F. and L.A. helped with sample collection; A.A. performed proteomic analysis; R.M. and D.C. helped with immunostaining; E.V. helped with sample collection; P.J. and D.B. helped with mini-gut experiments and edited the paper; C.S. coordinated research; F.F. and A.S. designed research and edited the paper; P.F. designed research, wrote and edited the paper.

Disclosure

The authors have nothing to disclose.

[14]Department of Internal Medicine, Obesity and Comorbidities Research Center (O.C.R.C.), State University of Campinas, São Paulo 13100, Brazil.

[#] These authors contributed equally to this work.

Summary

The role of circulating factors in regulating colonic stem cells (CoSCs) and colonic epithelial homeostasis is unclear. Individuals with long-standing type 1 diabetes (T1D) frequently have intestinal symptoms, termed diabetic enteropathy (DE), though its etiology is unknown. Here, we report T1D patients with DE exhibit abnormalities in their intestinal mucosa and CoSCs, which fail to generate in vitro mini-guts. Proteomic profiling of T1D+DE patient serum revealed altered levels of insulin-like growth factor 1 (IGF-1) and its binding protein-3 (IGFBP3). IGFBP3 prevented in vitro growth of patient-derived organoids via binding its receptor TMEM219, in an IGF-1-independent manner, and disrupted in vivo CoSC function in a preclinical DE model. Restoration of normoglycemia in patients with long-standing T1D via kidney-pancreas transplantation or in diabetic mice by treatment with an ecto-TMEM219 recombinant protein normalized circulating IGF-1/IGFBP3 levels and reestablished CoSC homeostasis. These findings demonstrate that peripheral IGF-1/IGFBP3 control CoSCs and their dysfunction in DE.

Keywords

colonic stem cells; IGF-I; IGFBP3; type 1 diabetes; type 2 diabetes; diabetic enteropathy; hyperglycemia; uremia; kidney transplantation; pancreas transplantation; diabetic nephropathy

Introduction

Gastrointestinal disorders, consisting of gastroparesis, abdominal distension, irritable bowel syndrome and fecal incontinence, are common in individuals with type 1 diabetes (T1D) (1993). Indeed up to 80% of individuals with long-standing T1D, who are generally affected by several diabetic complications including end stage renal disease (ESRD)(1993; Atkinson et al., 2013; Fiorina et al., 2001), show intestinal symptoms. The presence of these gastrointestinal symptoms, known as diabetic enteropathy (DE), significantly reduces the quality of life(1993; Atkinson et al., 2013; Camilleri, 2007; Talley et al., 2001) and has a largely unknown pathogenesis(Feldman and Schiller, 1983). Preclinical studies showed significant derangement of the intestinal mucosa morphology in diabetic rodents(Domenech et al., 2011; Zhao et al., 2003), suggesting that in T1D intestinal homeostasis may be altered; however, little data are available in humans. The intestinal epithelium is maintained by intestinal stem cells and their niche, which respond to physiological stress and to environmental injury(Barker, 2014; Medema and Vermeulen, 2011). Colonic stem cells (CoSCs), located at the crypt base of the large intestine and expressing the ephrin B receptor 2 (EphB2), leucine-rich repeat containing G protein-coupled receptor 5 (LGR5), h-TERT and aldehyde dehydrogenase (Aldh), among other markers(Carlone and Breault, 2012; Carpentino et al., 2009; Jung et al., 2011; Sato and Clevers, 2013), constitute, together with the local microenvironment, the CoSC niche (van der Flier and Clevers, 2009; Zeki et al., 2011). Recent studies have established conditions that recapitulate many features of

intestinal homeostasis and generate normal self-renewing crypt organoids *in vitro*, or so-called “mini-guts” (Jung et al., 2011; Sato and Clevers, 2013; Sato et al., 2011). Whether systemic factors, such as circulating hormones, serve to control CoSCs remains to be established(Stange and Clevers, 2013). We hypothesize that a dyad consisting of a circulating enterotrophic regulating factor and its binding protein (insulin-like growth factor 1, IGF-I, and its binding protein 3, IGFBP3) finely controls CoSCs and becomes dysfunctional in DE. Here we demonstrate that individuals with longstanding T1D and DE have altered CoSCs and show increased circulating levels of IGFBP3. Administration of IGFBP3 alters CoSC self-renewal potential and mucosal morphology *in vitro* and *in vivo,* in a preclinical model of DE, by quenching circulating IGF-I and by exerting a TMEM219-dependent/caspase-mediated toxic effect on CoSCs. Finally, targeting IGFBP3 with the newly generated ecto-TMEM219 recombinant protein, based on the extracellular domain of the IGFBP3 receptor (TMEM219), abrogates IGFBP3 deleterious effects *in vitro* and *in vivo.*

Results

Intestinal dysfunction and clinical symptoms are present in long-standing T1D

We first characterized intestinal morphology and function in a population of individuals with long-standing T1D and end stage renal disease (T1D+ESRD) and in healthy subjects (CTRL). Severe intestinal symptoms, such as diarrhea, abdominal pain and constipation were evident in T1D+ESRD individuals as assessed using the Gastrointestinal Symptom Rating Scale (GSRS) questionnaire (Fig. 1: A-C). Symptoms were associated with abnormalities in anorectal sphincter function (Fig. 1: D-F). The intestinal mucosa was altered in individuals with T1D+ESRD as compared to healthy subjects, with lower number of crypts, distortion and zonal sclerosis of the lamina propria (Fig. 1: G1-G2, H). A significant reduction in epithelial cell proliferation as assessed by Ki67 (MIB1 antibody) staining (Fig. 1: I1-I2, J), signs of neural degeneration and reduction in serotonin expression in intestinal neuroendocrine cells (Fig. 1: K1-K2, L, M1-M2, N) were observed, confirming the presence of DE in these individuals.

CoSCs are altered in long-standing T1D

The characterization of colonic crypts revealed a significant reduction in $EphB2^{+}$ expression andin the number of aldehyde dehydrogenase $(Aldh)^{+}$ immunoreactive cells, both markers of local stem cells(Carpentino et al., 2009; Jung et al., 2011), in T1D+ESRD individuals as compared to healthy subjects (Fig. 1: O1-O2, P, Q1-Q2, R). A profound decrease was evident, upon gating on viable cells at FACS analysis (Fig. S1: A-C), in the percentage of $EphB2^{hi}$, $EphB2^{hi+}LGR5^{+}$ and $EphB2^{+}$h-$TERT^{+}$ cells isolated from intestinal crypts obtained from T1D+ESRD individuals as compared to healthy subjects (Fig. 2: A-B, C-E, Fig. S1: D-E) and was confirmed by RT-PCR (Fig. 2: F-H) and western blot (WB) analysis (Fig. S1F). Transcriptome profiling of crypts obtained from T1D+ESRD documented decreased expression in Notch pathway (Notch1 and 2, JAG1, Dll1, Sox1 and 2), Wnt pathway (APC, FZD1, DKC1, ETS2, FAM84A, GPX2, RNF43) and BMP pathway (BMP1, BMP2, BMP3) genes, previously known pathways that control CoSCs, as compared to the expression of these genes in healthy subjects (Fig. S1G and Table S1). Analysis of CoSC

signature genes revealed that LGR5, EphB2(Gracz et al., 2013; Merlos-Suarez et al., 2011), h-TERT(Breault et al., 2008) and other intestinal stem cell marker genes(Hughes et al., 2011; Munoz et al., 2012; Ziskin et al., 2013) were significantly underexpressed in T1D +ESRD as compared to healthy subjects as well (Fig. 2I), confirming that CoSCs are altered in individuals with DE.

In vitro generation of mini-guts is altered in long-standing T1D

In order to evaluate CoSC self-renewal properties, we used the *in vitro* mini-gut assay. Indeed, crypts isolated from T1D+ESRD individuals and cultured *in vitro* for 8 days formed small spheroid mini-guts that failed to grow as compared to healthy subjects (Fig. 2: J1, J2, K), despite a comparable viability (Fig. S1: H-I) and efficiency of forming mini-guts in both groups (Fig. S1J). To begin to elucidate the effect of circulating factors and high glucose on CoSCs, we cultured isolated intestinal crypts obtained from healthy subjects in high glucose with/without serum obtained from long-standing T1D individuals *in vitro* for 8 days (Fig. 2: L1-L4, M). High glucose partially prevented the generation of fully mature mini-guts and synergized with serum of long-standing T1D individuals in altering CoSC self-renewal properties, such that mini-guts appeared collapsed (Fig. 2: L2-L4). Analysis of gene expression also revealed changes in the CoSC signature (Fig. 2N), thus suggesting that hyperglycemia and circulating factors act together to alter CoSC self-renewal properties in long-standing T1D.

Serum unbiased proteomic profiling revealed increased levels of IGFBP3 in long-standing T1D

In order to identify potential circulating factors that may serve as enterotrophic hormones and may have a role in regulating CoSCs, we compared the serum proteome of healthy subjects with T1D+ESRD individuals using an unbiased proteomic approach. A clear proteomic profile was evident in T1D+ESRD individuals as compared to healthy subjects, with more than 50% of the detected proteins segregating in either one group or the other (Fig. 3A). Some proteins were associated with diabetes, and some were growth factors or stem cell-related proteins or were potentially involved in intestinal functions (Fig. 3A). In particular, the levels of IGF-I binding proteins (IGFBP2 and 3) were detectable in long-standing T1D individuals as compared to healthy subjects, with IGFBP3 almost 5-fold increased (Fig. 3B), while IGFBP1, 4, 5 and 6 remained almost undetectable. Interestingly, in the liver of individuals with long-standing T1D, hepatocytes, but not Kupffer cells, showed a higher IGFBP3 immunohistochemical expression as compared to healthy subjects (Fig. 3: C1-C2, Fig. S1: K, L1-L6), suggesting an increase in IGFBP3 hepatic synthesis and release. The effect of high glucose on IGFBP3 hepatic release was confirmed by the detection of increased IGFBP3 levels in the supernatant of human immortalized hepatocytes exposed to high glucose (Fig. 3D). Finally, serum levels of free IGF-I appeared significantly reduced in long-standing T1D as compared to healthy subjects (Fig. 3E), indicating that circulating IGF-I and IGFBP3 levels are altered in long-standing T1D.

Peripheral IGFBP3 and IGF-I control CoSCs

To further elucidate the role of circulating IGF-I and IGFBP3 in the regulation of the CoSCs and of intestinal epithelial proliferation, we demonstrated the expression of IGF-IR and of

IGFBP3 receptor (TMEM219) on isolated crypts (Fig. 3: F, G1-G2, H, Fig. S1: M, N1-N2) using RT-PCR and WB, and confirmed the expression of IGF-IR on CoSCs with immunostaining (Fig. S1: N1-N2), and of TMEM219 with in situ hybridization (Fig. 3: G1-G2). In order to mechanistically confirm the role of IGF-I and IGFBP3 on CoSCs, we tested the effect of several molecules, identified by proteomic profiling, in our *in vitro* mini-gut assay. Our strategy to select potential targets is reported in Supplemental Information. The severely altered mini-guts generated from intestinal samples obtained from T1D+ESRD individuals were rescued by the addition of recombinant human IGF-I (IGF-I) to the culture medium (Fig. 3I), while the addition of recombinant human IGFBP3 (IGFBP3) resulted in the abrogation of the positive effect observed with IGF-I, with a decreased development of mini-guts and increased formation of collapsed and distorted organoids (Fig. 3I). Because IGFBP3 has been recently shown to act independently of IGF-I(Williams et al., 2007) via the IGFBP3 receptor (TMEM219)(Baxter, 2013), it was necessary to clarify whether IGFBP3 exerts its effects on CoSCs by binding IGF-I or by directly targeting TMEM219 on CoSCs. We first confirmed that IGFBP3 has a direct pro-apoptotic effect on CoSCs by demonstrating increased Caspase 8 and 9 expression in mini-guts obtained from healthy subjects and long-standing T1D individuals and cultured with IGFBP3 (Fig. 3J, Fig. S2: A-B), while the addition of a Pan-Caspase inhibitor (Z-VAD-FMK) or the addition of both selective inhibitors of Caspases 8 and 9, but not that of Caspase 3 inhibitor, abrogated the IGFBP3 effect (Fig. 3K). We then demonstrated that the addition of IGF-I did not rescue the development of mini-guts obtained from healthy subjects and exposed to IGFBP3 (Fig. 3L), confirming that IGFBP3 may act through both a direct and indirect IGF-I mechanism. Interestingly, high glucose alone was unable to completely disrupt mini-gut growth, and anti-IGF-IR did not worsen growth and morphology of mini-guts formed from healthy subjects (Fig. 3L). The addition of IGF-I to mini-guts generated from healthy subjects, but cultured with high glucose and serum from long-standing T1D individuals, rescued mini-gut morphology, while IGFBP3 abolished the positive effect of IGF-I when added to the mini-gut culture (Fig. 3L). Interestingly, the use of healthy subjects' "CTRL" serum in culturing crypts obtained from longstanding T1D nearly restored mini-gut development/morphology, indicating that circulating factors, and in particular the IGF-I/IGFBP3 dyad, control CoSCs (Fig. S2: C-D). We then genetically modulated TMEM219 expression by using siRNA *in vitro* in mini-guts obtained from healthy subjects. Knockdown of TMEM219 in mini-guts preserved their ability to grow and self-renew, despite the addition of IGFBP3 and high glucose with long-standing T1D serum (Fig. 3M). Concomitant blockade of TMEM219 by siRNA and of IGF-IR by antibody blockade did not result in any additional beneficial effect on mini-gut development despite using serum from healthy subjects or from long-standing T1D (Fig. S2E).

Other circulating proteins that appeared altered in the serum proteome of long-standing T1D individuals were tested in the *in vitro* mini-gut assay and did not show any significant effect on mini-gut growth (Fig. S2: F-G). C-peptide and insulin, which are commonly altered in T1D and which may interfere with IGF-I/IGFBP3 dyad by binding IGF-IR (Fig. S2: F, H), were tested as well and did not show any effect.

To further confirm that IGF-I/IGFBP3 dyad effectively targets CoSCs and not only crypts, we tested IGF-I/IGFBP3 effect on single cell-derived mini-guts. We flow-sorted $EphB2^{+}$

cells from isolated crypts and established that TMEM219 was highly expressed on their surface (Fig. 4A). We then cultured EphB2^{+} cells in the *in vitro* single cell-derived mini-gut assay and confirmed that high glucose and long-standing T1D serum exposure as well as addition of IGFBP3 significantly abrogated single cell-derived mini-gut growth, thus recapitulating the primary features reported in our previous observations on crypt-derived mini-guts (Fig. 4B, Fig. S3: A1-A3). Moreover, expression of Caspases 8 and 9 was up-regulated in IGFBP3-treated mini-guts and in those exposed to high glucose and long-standing T1D serum, while Ki67, a marker of proliferation, was significantly under-expressed (Fig. S3: B-D).

Effect of the IGF-I/IGFBP3 dyad on previously known pathways that control CoSCs

In order to clarify the effects of the IGF-I/IGFBP3 dyad on pathways previously known to be involved in CoSC niche function (i.e. Wnt/Notch/BMP), we obtained from our stem cell transcriptome profile the expression of niche regulating specific gene transcripts. IGF-I restores the expression of some factors associated with Wnt/Notch signaling pathways on mini-guts obtained from crypts of T1D+ESRD (Fig. S3E, Table S2), while IGFBP3 poorly affects Wnt/Notch/BMP gene expression in mini-guts obtained from crypts of healthy subjects or from those obtained from T1D+ESRD individuals (Fig. S3F, Table S2). This confirms that IGF-I preserves the expression of some genes involved in Wnt/Notch/BMP signaling, but also that IGFBP3 acts independently on CoSCs, without major alterations in the expression of key target genes of the other previously known pathways.

Effect of the IGF-I/IGFBP3 dyad on apoptotic pathways

An extensive transcriptome analysis performed to clarify the IGFBP3 caspase-mediated effect on mini-guts (Fig. 4: C-D, Fig. S3: G-H, Table S3) showed that addition of IGFBP3 to mini-guts grown from healthy subject crypts was associated with a significant up-regulation of caspase cascade activators (Caspases 8 and 9) and pro-apoptotic genes, while the anti-apoptotic gene Bcl2 was down-regulated (Fig. 4C). Interestingly, anti-apoptotic genes (Bcl2, Fas, Nol3) were significantly underexpressed in mini-guts grown from T1D+ESRD crypts as well, as compared to healthy subjects, while the majority of caspase related genes (Caspase 1, 5, 7, 8, 9, 14) were over-expressed (Fig. S3G). Moreover, the expression of genes involved in other pro-apoptotic pathways was either not altered (i.e. FasL, FADD, TNF) or inhibited (TRADD) in T1D+ESRD mini-guts. The opposite effect was observed by adding IGF-I (Fig. 4D, Fig. S3H). The absence of alterations in the expression of oxidative stress target genes (data not shown), and of any effect of oxidative stress factors (Figure S3: I-J), confirmed apoptotic-related caspase-mediated IGFBP3 activity. The expression of the survival factor beta-catenin (CTNNB1) was reduced in mini-guts generated from crypts of T1D+ESRD individuals as compared to those obtained from healthy subjects (Fig. S3K) and was increased by the addition of IGF-I (Fig. S3L), further supporting the concept of an apoptotic-related mechanism, whereby circulating IGFBP3 directly controls CoSCs (Video S1).

Manipulation of the circulating IGF-I/IGFBP3 dyad alters the course of diabetic enteropathy in a preclinical model

In order to further demonstrate the relevance of IGF-I/IGFBP3 circulating factors *in vivo*, we tested the effects of IGF-I and IGFBP3 administration in a preclinical model of DE. After 8 weeks of chemically-induced diabetes (using streptozotocin [STZ]), C57BL/6 (B6) mice showed a reduced number of crypts in the colorectal tissue (Fig. 4E), which displayed increased depth (Fig. 4F) and width in more than 70% of cases (Fig. 4G, I1-I2, I4-I5) and a reduced number of $Aldh^+$ cells (Fig. 4H, J1-J2). Interestingly, these mice showed increased serum levels of IGFBP3 and low levels of IGF-I, with lower murine insulin levels as compared to naïve B6 (Fig. S4: A-C). Intraperitoneal (i.p.) administration of IGFBP3 in naïve B6 mice resulted in a reduction in local crypt numbers (Fig. 4: E, I3), with the majority of crypts showing increased depth and width (Fig. 4: F, G, I3, I6) and significant reduction in $Aldh^+$ cells as compared to untreated mice (Fig. 4: H, J3). Those features were aggravated by IGFBP3 administration to STZ-treated B6 mice (Fig. S4: D-G, H1-H2), with evidence of decreases in weight (Fig. S4I), CoSC loss (Fig. S4: J-L) and up-regulated expression of Caspases 8 and 9 (Fig. S4: M-N). Administration of IGF-I i.p in STZ-treated B6 mice only partially improved mucosa morphology increased number of normal crypts, which remained abnormal (Fig. S4D, H1-H2), and only partially restored the number of $Aldh^+$ cells (Fig. S4G). Validation for successful administration of the injected compounds was performed by analyzing IGF-I/IGFBP3 peripheral levels after 1-hour injection (Fig. S4: O-P).These observations confirmed that peripheral IGF-I/IGFBP3 dyad controls CoSCs (Fig. 4K).

Treatment of long-standing T1D with simultaneous pancreas-kidney transplantation (SPK) reverts clinical and morphological features of DE

The gold standard treatment for long-standing T1D is SPK, which affords stable glycometabolic control, near-normalize risk factors and prolonged survival (Table S4) (Fiorina et al., 2004; Fiorina et al., 2005; Folli et al., 2010; Secchi et al., 1998; Smets et al., 1999). However, individuals with T1D+ESRD are also treated with kidney transplantation alone but remain diabetic (K+T1D)(Fiorina et al., 2001). A significant improvement in gastrointestinal symptoms was evident over time after SPK in our cohort of transplanted individuals, while the K+T1D group did not report any benefit (Fig. S5: A-C), suggesting that DE is reversible.

Treatment of long-standing T1D with SPK re-establishes intestinal mucosa morphology and local self-renewal properties

Analysis of intestinal mucosa samples showed a significant recovery in the structure of the epithelial compartment, with compensatory epithelial hyperplasia in the SPK group (Fig. S5: D1-D2). Recovery of normal crypt histology and number was evident in the SPK group when longstanding T1D was successfully treated while none of these features were evident in individuals who received kidney transplant only and remained diabetic (Fig. S5: D1-D2). Epithelial cell proliferation ($MIB1^+$ cells) increased after SPK over time as compared to baseline and to K+T1D at each timepoint (Fig. 4: L, M1-M2), with near-normalization of intestinal morphology, epithelial renewal and neural features (Fig. S5: E1-E2, F, G1-G2, H-I,

J1-J2, K). This demonstrates that treatment of long-standing T1D with SPK promoted recovery of intestinal epithelial repair and of self-renewing properties.

Treatment of long-standing T1D promotes restoration of CoSCs

Treatment of long-standing T1D with SPK is associated with an increase in $Aldh^+$ cells (Fig. 4: N, O1-O2) and $EphB2^+$ expression in the intestinal crypt (Fig. 4: P, Q1-Q2) and nearly normalizes the percentage of $EphB2^{hi+}$, $EphB2^+hTERT^+$ and $EphB2^{hi+}LGR5^+$ cells in isolated intestinal crypts as compared to baseline (Fig. 5: A-C). CoSC marker expression (Fig. 5: D-G) and growth/morphology of mini-guts obtained from SPK individuals were nearly normalized as well (Fig. 5H, Fig. S6: A1-A6). Transcriptome analysis revealed that SPK nearly restored the expression of CoSCs markers and of pathways involved in preserving CoSCs integrity (Fig. 5I, Fig. S6B). Taken together, our data suggest that treatment of long-standing T1D with SPK promotes restoration of CoSCs.

Treatment of long-standing T1D with SPK restores circulating IGF-I and IGFBP3

Broad proteomic analysis and targeted immunoassay, revealed a near-normalization of IGFBP3 and IGF-I serum levels after SPK (Fig. 5: J-K) in association with a nearly re-established expression of IGF-IR (Fig. S6C). These results were not evident in the K+T1D group, who showed low levels of IGF-I (Fig. 5J) and IGF-IR expression (Fig. S6C) and only a partial recovery in their IGFBP profile (Fig. S6D). A significant correlation between IGFBP3 serum levels and intestinal symptoms in both SPK and K+T1D groups, but more evident in the latter, confirmed that the restoration of IGFBP3 levels is associated with an improvement in diabetic enteropathy (Fig. 5: L-M). Treatment of long-standing T1D with SPK ameliorates diabetic enteropathy via a glucose-associated restoration of the circulating IGF-I/IGFBP3 dyad.

The ecto-TMEM219 recombinant protein abrogates IGFBP3-mediated mini-gut destruction in vitro and preserves CoSCs in vivo in a murine model of DE

In order to further demonstrate the IGFBP3-mediated detrimental effects on CoSCs, we generated a recombinant protein based on the 161-amino-acid TMEM219 extracellular domain (ecto-TMEM219), with >90% purity. Addition of ecto-TMEM219 (2:1 molar ratio with IGFBP3) to crypts obtained from CTRL and cultured with IGFBP3 abrogated the pro-apoptotic effect of IGFBP3 on mini-guts and preserved the regenerative properties of crypts to generate mini-guts (Fig. 6A). The expression of CoSC marker EphB2 was significantly recovered in mini-guts cultured with IGFBP3 and ecto-TMEM219 (Fig. 6B), emphasizing a favorable effect in preserving CoSCs, which was also confirmed in high glucose-cultured mini-guts (Fig. 6A). Moreover, analysis of Caspases 8 and 9 by RT-PCR documented a net decrease in their expression when ecto-TMEM219 was added to IGFBP3-cultured mini-guts as compared to IGFBP3 alone (Fig. 6: C-D). We then treated STZ-B6 mice with ecto-TMEM219 and observed improved mucosa morphology with recovered number, depth and width of crypts (Fig. 6: E-G). Administration of ecto-TMEM219 was associated with an increase in mouse body weight as compared to STZ-treated B6 (Fig. 6H), with significant regain of CoSCs (Fig. 6: I-K), a decreased expression of Caspases 8 and 9 (Fig. 6: L-M) and a re-establishment of circulating IGFBP3 levels (Fig. 6N), therefore suggesting a curative potential of ecto-TMEM219 in a therapeutic scenario.

Discussion

Diabetic enteropathy represents a clinically relevant complication in individuals with T1D, as it is associated with lower quality of life, malnutrition and malabsorbtion(Bytzer et al., 2002; Faraj et al., 2007; Talley et al., 2001). Particularly, in individuals with long-standing T1D (T1D+ESRD), intestinal disorders occur with high frequency and severity(Cano et al., 2007; Wu et al., 2004), resulting in body mass loss and cachexia(Pupim et al., 2005), indicating that enteropathy is an important complication of long-standing T1D(Atkinson et al., 2013; Pambianco et al., 2006). Our results demonstrate that individuals with long-standing T1D experienced severe intestinal disorders and that these clinical conditions are associated with alterations of the intestinal mucosa, with reduced proliferation of intestinal epithelial cells and with signs of neural degeneration. Similar features have also been reported in rodent models of T1D and DE(Domenech et al., 2011). Our data link DE to a defect in CoSCs and implicate IGFBP3 as having an important role in the maintenance of intestinal epithelium homeostasis. While hyperglycemia is a prominent feature of T1D, our *in vitro* studies suggest that this feature cannot fully explain DE and that circulating factors may play an important role. Proteomic analysis led to the identification of IGF-I as an enterotrophic factor involved in the homeostasis of CoSCs. We then confirmed that IGF-I and IGFBP3 control CoSCs and that this axis is dysfunctional in long-standing T1D. Our data indicate that IGF-I acts as a circulating enterotrophic factor that promotes crypt growth and controls CoSCs through IGF-IR, while IGFBP3 can block IGF-I signaling by binding circulating IGF-I and reducing its bioavailability. In addition, and most importantly, we showed that IGFBP3 acts through a pro-apoptotic IGF-I-independent mechanism on CoSCs, which we demonstrated express TMEM219 (the IGFBP3 receptor), thereby inducing the failure of mini-gut growth. This latter effect is Caspase 8- and 9-mediated and TMEM219-dependent; indeed, the absence of the IGFBP3 receptor (TMEM219) on CoSCs greatly diminished high glucose-associated CoSC injuries. T1D together with starvation and cachexia are characterized by low circulating IGF-I levels(Bondy et al., 1994; Giustina et al., 2014) due to reduced hepatic IGF-I release, which is controlled and stimulated by endogenous insulin(Le Roith, 1997; Sridhar and Goodwin, 2009). More importantly, hyperglycemia appeared to have a direct effect on hepatic synthesis and release of IGFBP3. IGFBP3 may thus act as a hepatic hormone that reduces intestinal absorptive capacity during hyperglycemia. Interestingly, SPK provided a proof of concept to our hypothesis and supported our findings regarding the existence of circulating factors that control CoSCs. The striking improvement of clinical and functional features of DE that we observed in our study, associated with replenishment of CoSCs and with restoration of the circulating IGF-I and IGFBP3, strengthens our hypothesis. Finally, the newly generated ecto-TMEM219 recombinant protein improved DE in diabetic mice *in vivo* and restored the ability of mini-guts to grow normally *in vitro*, thus confirming the role of IGFBP3 in controlling CoSCs and paving the way for a potential therapeutic strategy (Video S1). In summary, our study shows that an IGFBP3-mediated disruption of CoSCs linked to hyperglycemia is evident in DE. We suggest that circulating IGF-I/IGFBP3 represent a hormonal dyad that controls CoSCs and a therapeutic target for individuals with intestinal disorders caused by diabetes mellitus of long duration (Bondy et al., 1994; Bortvedt and Lund, 2012; Boucher et al., 2010).

Experimental Procedure

60 individuals with long-standing T1D (T1D+ESRD) registered on the waiting list for simultaneous pancreas-kidney transplantation (SPK) were enrolled in the study and compared with 20 healthy subjects matched for age and gender (CTRL). Assessment of gastrointestinal symptoms, intestinal motility and intestinal mucosa pathology defined DE. CoSCs were identified on colonic purified crypts based on the expression of CoSC specific markers (flow cytometry, RT-PCR, western blot, transcriptome profiling). CoSC self-renewal properties were assessed by evaluating the percentage of *in vitro* developed mini-guts and by characterizing their expression of cell lineage markers in different conditions (Fig. S6: E-I, J). Interventional studies included the use of recombinant human IGF-I, recombinant human IGFBP3 and anti-IGF-IR *in vitro* in mini-gut assay and *in vivo* in murine models of DE. Animal studies were conducted on C57BL/6 (B6) mice purchased from the Jackson Laboratory (Bar Harbor, Maine), in accordance with institutional guidelines (Harvard Medical School Institutional Animal Care and Use Committee). Mice were rendered diabetic with streptozotocin injection and development of DE was assessed after 8 weeks (intestinal pathology, CoSCs flow cytometry and RT-PCR). The recombinant protein ecto-TMEM219 for *in vitro* and *in vivo* studies (161 amino acids, 18.2 kDa) was generated using *E. coli* for expression and synthesis, while purity was tested by SDS-PAGE and WB (Fig. S6: K-L). The co-injection of IGFBP3 and ecto-TMEM219 prevented the increase of IGFBP3 peripheral levels and implies the binding of ecto-TMEM219 with IGFBP3 (Fig. S6M). Broad serum proteomic analysis was used to detect circulating factors that may regulate CoSCs and candidate factors were then tested in the *in vitro* mini-gut assay (Table S5). Peripheral levels of IGF-I and IGFBP3 were confirmed in human and murine studies using targeted immunoassays. Detailed methods and statistical analysis are described in the Supplemental Information. The Study was approved by the Institutional Review Board of Istituto di Ricovero e Cura a Carattere Scientifico Ospedale San Raffaele, Milano, Italy (Enteropathy-Pancreas KidneyTransplantation/01 Secchi/Fiorina).

Supplementary Material

Refer to Web version on PubMed Central for supplementary material.

Acknowledgments

We thank Protein Micro Sequncing Facility, Ospedale San Raffaele, Milan, Italy for proteomic analysis, and Gabriella Becchi (Department of Biomedical, Biotechnological and Translational Sciences, Unit of Pathology, University of Parma, Parma) for immunohistochemistry studies. Francesca D'Addio is a recipient of an Italian Scientists and Scholars of North America Foundation (ISSNAF)-Fondazione Marche Fellowship. Paolo Fiorina, Carlo Staudacher and Antonio Secchi are recipients of a Minister of Health of Italy grant RF-2010-2314794. Paolo Fiorina received a Minister of Health of Italy grant RF-2010-233119. Paolo Fiorina is the recipient of an ADA mentor-based fellowship and of an EFSD/Sanofi European Research Programme and is supported by an American Heart Association (AHA) Grant-in-Aid. Roberto Bassi is supported by an AST fellowship. Moufida Ben Nasr is supported by an ADA mentor-based fellowship. David Breault is supported by RO1DK084056 and P30DK034854. Franco Follli is supported by FAPESP, CNPq and the University of Campinas, São Paulo, Brazil.

References

The effect of intensive treatment of diabetes on the development and progression of long-term complications in insulin-dependent diabetes mellitus. The Diabetes Control and Complications Trial Research Group. N Engl J Med. 1993; 329:977–986. [PubMed: 8366922]

Atkinson MA, Eisenbarth GS, Michels AW. Type 1 diabetes. Lancet. 2013

Barker N. Adult intestinal stem cells: critical drivers of epithelial homeostasis and regeneration. Nat Rev Mol Cell Biol. 2014; 15:19–33. [PubMed: 24326621]

Baxter RC. Insulin-like growth factor binding protein-3 (IGFBP-3): Novel ligands mediate unexpected functions. J Cell Commun Signal. 2013; 7:179–189. [PubMed: 23700234]

Bondy CA, Underwood LE, Clemmons DR, Guler HP, Bach MA, Skarulis M. Clinical uses of insulin-like growth factor I. Ann Intern Med. 1994; 120:593–601. [PubMed: 8116999]

Bortvedt SF, Lund PK. Insulin-like growth factor 1: common mediator of multiple enterotrophic hormones and growth factors. Curr Opin Gastroenterol. 2012; 28:89–98. [PubMed: 22241077]

Boucher J, Macotela Y, Bezy O, Mori MA, Kriauciunas K, Kahn CR. A kinase-independent role for unoccupied insulin and IGF-1 receptors in the control of apoptosis. Sci Signal. 2010; 3:ra87. [PubMed: 21139139]

Breault DT, Min IM, Carlone DL, Farilla LG, Ambruzs DM, Henderson DE, Algra S, Montgomery RK, Wagers AJ, Hole N. Generation of mTert-GFP mice as a model to identify and study tissue progenitor cells. Proc Natl Acad Sci U S A. 2008; 105:10420–10425. [PubMed: 18650388]

Bytzer P, Talley NJ, Hammer J, Young LJ, Jones MP, Horowitz M. GI symptoms in diabetes mellitus are associated with both poor glycemic control and diabetic complications. Am J Gastroenterol. 2002; 97:604–611. [PubMed: 11922554]

Camilleri M. Clinical practice. Diabetic gastroparesis. N Engl J Med. 2007; 356:820–829. [PubMed: 17314341]

Cano AE, Neil AK, Kang JY, Barnabas A, Eastwood JB, Nelson SR, Hartley I, Maxwell D. Gastrointestinal symptoms in patients with end-stage renal disease undergoing treatment by hemodialysis or peritoneal dialysis. Am J Gastroenterol. 2007; 102:1990–1997. [PubMed: 17511755]

Carlone DL, Breault DT. Tales from the crypt: the expanding role of slow cycling intestinal stem cells. Cell Stem Cell. 2012; 10:2–4. [PubMed: 22226346]

Carpentino JE, Hynes MJ, Appelman HD, Zheng T, Steindler DA, Scott EW, Huang EH. Aldehyde dehydrogenase-expressing colon stem cells contribute to tumorigenesis in the transition from colitis to cancer. Cancer Res. 2009; 69:8208–8215. [PubMed: 19808966]

Domenech A, Pasquinelli G, De Giorgio R, Gori A, Bosch F, Pumarola M, Jimenez M. Morphofunctional changes underlying intestinal dysmotility in diabetic RIP-I/hIFNbeta transgenic mice. Int J Exp Pathol. 2011; 92:400–412. [PubMed: 22050417]

Faraj J, Melander O, Sundkvist G, Olsson R, Thorsson O, Ekberg O, Ohlsson B. Oesophageal dysmotility, delayed gastric emptying and gastrointestinal symptoms in patients with diabetes mellitus. Diabet Med. 2007; 24:1235–1239. [PubMed: 17725632]

Feldman M, Schiller LR. Disorders of gastrointestinal motility associated with diabetes mellitus. Ann Intern Med. 1983; 98:378–384. [PubMed: 6402969]

Fiorina P, Folli F, D'Angelo A, Finzi G, Pellegatta F, Guzzi V, Fedeli C, Della Valle P, Usellini L, Placidi C, et al. Normalization of multiple hemostatic abnormalities in uremic type 1 diabetic patients after kidney-pancreas transplantation. Diabetes. 2004; 53:2291–2300. [PubMed: 15331538]

Fiorina P, La Rocca E, Venturini M, Minicucci F, Fermo I, Paroni R, D'Angelo A, Sblendido M, Di Carlo V, Cristallo M, et al. Effects of kidney-pancreas transplantation on atherosclerotic risk factors and endothelial function in patients with uremia and type 1 diabetes. Diabetes. 2001; 50:496–501. [PubMed: 11246868]

Fiorina P, Venturini M, Folli F, Losio C, Maffi P, Placidi C, La Rosa S, Orsenigo E, Socci C, Capella C, et al. Natural history of kidney graft survival, hypertrophy, and vascular function in end-stage renal disease type 1 diabetic kidney-transplanted patients: beneficial impact of pancreas and successful islet cotransplantation. Diabetes Care. 2005; 28:1303–1310. [PubMed: 15920043]

Folli F, Guzzi V, Perego L, Coletta DK, Finzi G, Placidi C, La Rosa S, Capella C, Socci C, Lauro D, et al. Proteomics reveals novel oxidative and glycolytic mechanisms in type 1 diabetic patients' skin which are normalized by kidney-pancreas transplantation. PLoS One. 2010; 5:e9923. [PubMed: 20360867]

Giustina A, Berardelli R, Gazzaruso C, Mazziotti G. Insulin and GH-IGF-I axis: endocrine pacer or endocrine disruptor? Acta Diabetol. 2014

Gracz AD, Fuller MK, Wang F, Li L, Stelzner M, Dunn JC, Martin MG, Magness ST. Brief Report: CD24 and CD44 mark human intestinal epithelial cell populations with characteristics of active and facultative stem cells. Stem Cells. 2013; 31:2024–2030. [PubMed: 23553902]

Hughes KR, Sablitzky F, Mahida YR. Expression profiling of Wnt family of genes in normal and inflammatory bowel disease primary human intestinal myofibroblasts and normal human colonic crypt epithelial cells. Inflamm Bowel Dis. 2011; 17:213–220. [PubMed: 20848536]

Jung P, Sato T, Merlos-Suarez A, Barriga FM, Iglesias M, Rossell D, Auer H, Gallardo M, Blasco MA, Sancho E, et al. Isolation and in vitro expansion of human colonic stem cells. Nat Med. 2011; 17:1225–1227. [PubMed: 21892181]

Le Roith D. Seminars in medicine of the Beth Israel Deaconess Medical Center. Insulin-like growth factors. N Engl J Med. 1997; 336:633–640. [PubMed: 9032050]

Medema JP, Vermeulen L. Microenvironmental regulation of stem cells in intestinal homeostasis and cancer. Nature. 2011; 474:318–326. [PubMed: 21677748]

Merlos-Suarez A, Barriga FM, Jung P, Iglesias M, Cespedes MV, Rossell D, Sevillano M, Hernando-Momblona X, da Silva-Diz V, Munoz P, et al. The intestinal stem cell signature identifies colorectal cancer stem cells and predicts disease relapse. Cell Stem Cell. 2011; 8:511–524. [PubMed: 21419747]

Munoz J, Stange DE, Schepers AG, van de Wetering M, Koo BK, Itzkovitz S, Volckmann R, Kung KS, Koster J, Radulescu S, et al. The Lgr5 intestinal stem cell signature: robust expression of proposed quiescent '+4' cell markers. EMBO J. 2012; 31:3079–3091. [PubMed: 22692129]

Pambianco G, Costacou T, Ellis D, Becker DJ, Klein R, Orchard TJ. The 30-year natural history of type 1 diabetes complications: the Pittsburgh Epidemiology of Diabetes Complications Study experience. Diabetes. 2006; 55:1463–1469. [PubMed: 16644706]

Pupim LB, Heimburger O, Qureshi AR, Ikizler TA, Stenvinkel P. Accelerated lean body mass loss in incident chronic dialysis patients with diabetes mellitus. Kidney Int. 2005; 68:2368–2374. [PubMed: 16221242]

Sato T, Clevers H. Growing self-organizing mini-guts from a single intestinal stem cell: mechanism and applications. Science. 2013; 340:1190–1194. [PubMed: 23744940]

Sato T, Stange DE, Ferrante M, Vries RG, Van Es JH, Van den Brink S, Van Houdt WJ, Pronk A, Van Gorp J, Siersema PD, et al. Long-term expansion of epithelial organoids from human colon, adenoma, adenocarcinoma, and Barrett's epithelium. Gastroenterology. 2011; 141:1762–1772. [PubMed: 21889923]

Secchi A, Caldara R, La Rocca E, Fiorina P, Di Carlo V. Cardiovascular disease and neoplasms after pancreas transplantation. Lancet. 1998; 352:65. author reply 66. [PubMed: 9800776]

Smets YF, Westendorp RG, van der Pijl JW, de Charro FT, Ringers J, de Fijter JW, Lemkes HH. Effect of simultaneous pancreas-kidney transplantation on mortality of patients with type-1 diabetes mellitus and end-stage renal failure. Lancet. 1999; 353:1915–1919. [PubMed: 10371569]

Sridhar SS, Goodwin PJ. Insulin-insulin-like growth factor axis and colon cancer. J Clin Oncol. 2009; 27:165–167. [PubMed: 19064959]

Stange DE, Clevers H. Concise review: the yin and yang of intestinal (cancer) stem cells and their progenitors. Stem Cells. 2013; 31:2287–2295. [PubMed: 23836510]

Talley NJ, Young L, Bytzer P, Hammer J, Leemon M, Jones M, Horowitz M. Impact of chronic gastrointestinal symptoms in diabetes mellitus on health-related quality of life. Am J Gastroenterol. 2001; 96:71–76. [PubMed: 11197290]

van der Flier LG, Clevers H. Stem cells, self-renewal, and differentiation in the intestinal epithelium. Annual review of physiology. 2009; 71:241–260.

Williams AC, Smartt H, AM HZ, Macfarlane M, Paraskeva C, Collard TJ. Insulin-like growth factor binding protein 3 (IGFBP-3) potentiates TRAIL-induced apoptosis of human colorectal carcinoma cells through inhibition of NF-kappaB. Cell Death Differ. 2007; 14:137–145. [PubMed: 16645643]

Wu MJ, Chang CS, Cheng CH, Chen CH, Lee WC, Hsu YH, Shu KH, Tang MJ. Colonic transit time in long-term dialysis patients. Am J Kidney Dis. 2004; 44:322–327. [PubMed: 15264191]

Zeki SS, Graham TA, Wright NA. Stem cells and their implications for colorectal cancer. Nature reviews. Gastroenterology & hepatology. 2011; 8:90–100. [PubMed: 21293509]

Zhao J, Yang J, Gregersen H. Biomechanical and morphometric intestinal remodelling during experimental diabetes in rats. Diabetologia. 2003; 46:1688–1697. [PubMed: 14593459]

Ziskin JL, Dunlap D, Yaylaoglu M, Fodor IK, Forrest WF, Patel R, Ge N, Hutchins GG, Pine JK, Quirke P, et al. In situ validation of an intestinal stem cell signature in colorectal cancer. Gut. 2013; 62:1012–1023. [PubMed: 22637696]

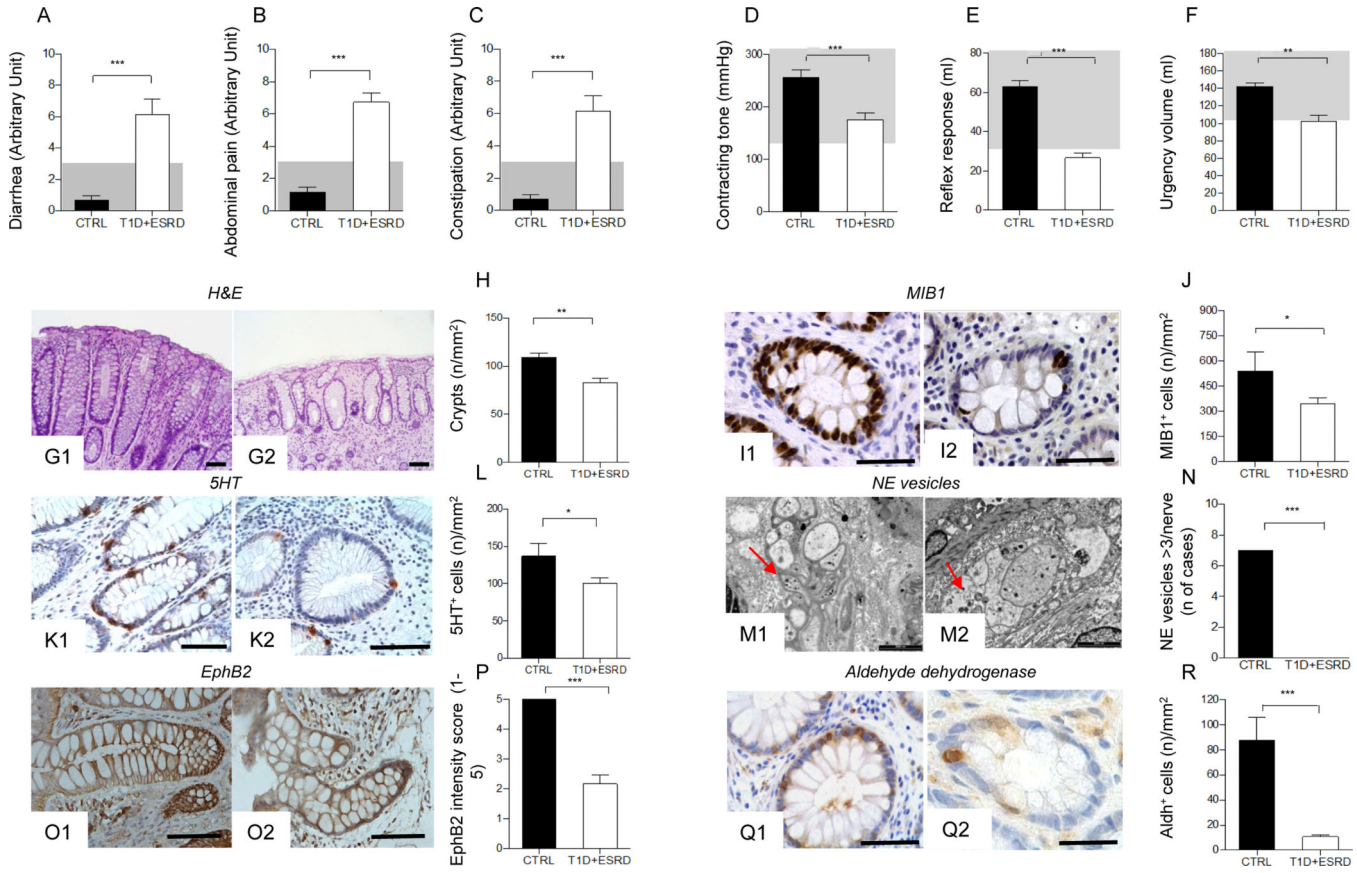

Figure 1. Diabetic enteropathy in long-standing T1D is characterized by intestinal mucosa abnormalities and impairment in colonic stem cells

A, B, C. Bar graphs depict the score of diarrhea, abdominal pain and constipation according to the administration of the GSRS questionnaire in healthy subjects (CTRL) and long-standing T1D individuals (T1D+ESRD). Gray area indicates normal range for the parameter. **D, E, F**. Bar graphs report the measurements of anorectal sphincter contracting tone (mmHg), reflex response (ml) and urgency volume (ml) by anorectal manometry in healthy subjects (CTRL) and longstanding T1D individuals (T1D+ESRD). Gray area indicates normal range for the parameter. n=20 CTRL and n=60 T1D+ESRD individuals were included in the evaluation. **G1-G2, I1-I2, K1-K2, M1-M2, O1-O2, Q1-Q2**. Representative images of hematoxylin and eosin (H&E) histology staining, immunoreactive Ki67^{+} cells (MIB1^{+}), ultrastructural analysis of neural structures with red arrows indicating localization and presence of neuroendocrine vesicles, immunohistochemical expression of 5HT, aldehyde dehydrogenase (Aldh)$^{+}$ cells, and EphB2^{+} expression, on bioptic samples obtained from healthy subjects (CTRL, G1, I1, K1, M1, O1, Q1) and long-standing T1D individuals (T1D+ESRD, G2, I2, K2, M2, O2, Q2). Ultrastructural analysis scale bar: 2000 nm. Original histology magnification: 100X in G1-G2; 400X in I1-I2, K1-K2; 40X in O1-O2; 200X, in Q1-Q2. Scale bar 80 micron. **H**, **J, L, N, P, R**. Bar graphs reporting the measurement of crypts, the number of Ki67^{+} (MIB1^{+}) cells, of neuroendocrine vesicles of nerve terminals (number of cases with >3 NE vesicles detected per nerve terminal), of 5HT^{+} and Aldh^{+} cells, and of EphB2^{+} expression (intensity score 0-5) in CTRL and long-standing T1D

subjects (T1D+ESRD). n=20 CTRL and n=60 T1D+ESRD individuals were included in the evaluation. Data are expressed as mean ± standard error of the mean (SEM) unless differently reported. *p<0.01; **p<0.001; ***p<0.0001.

Abbreviations: GSRS, Gastrointestinal Symptom Rating Scale; T1D, type 1 diabetes; ESRD, end stage renal disease; CTRL, healthy subjects; H&E, hematoxylin and eosin; MIB1, antibody against Ki67; EphB2, Ephrin B receptor 2; Aldh, Aldehyde dehydrogenase; 5HT, serotonin; NE, neuroendocrine vesicles.

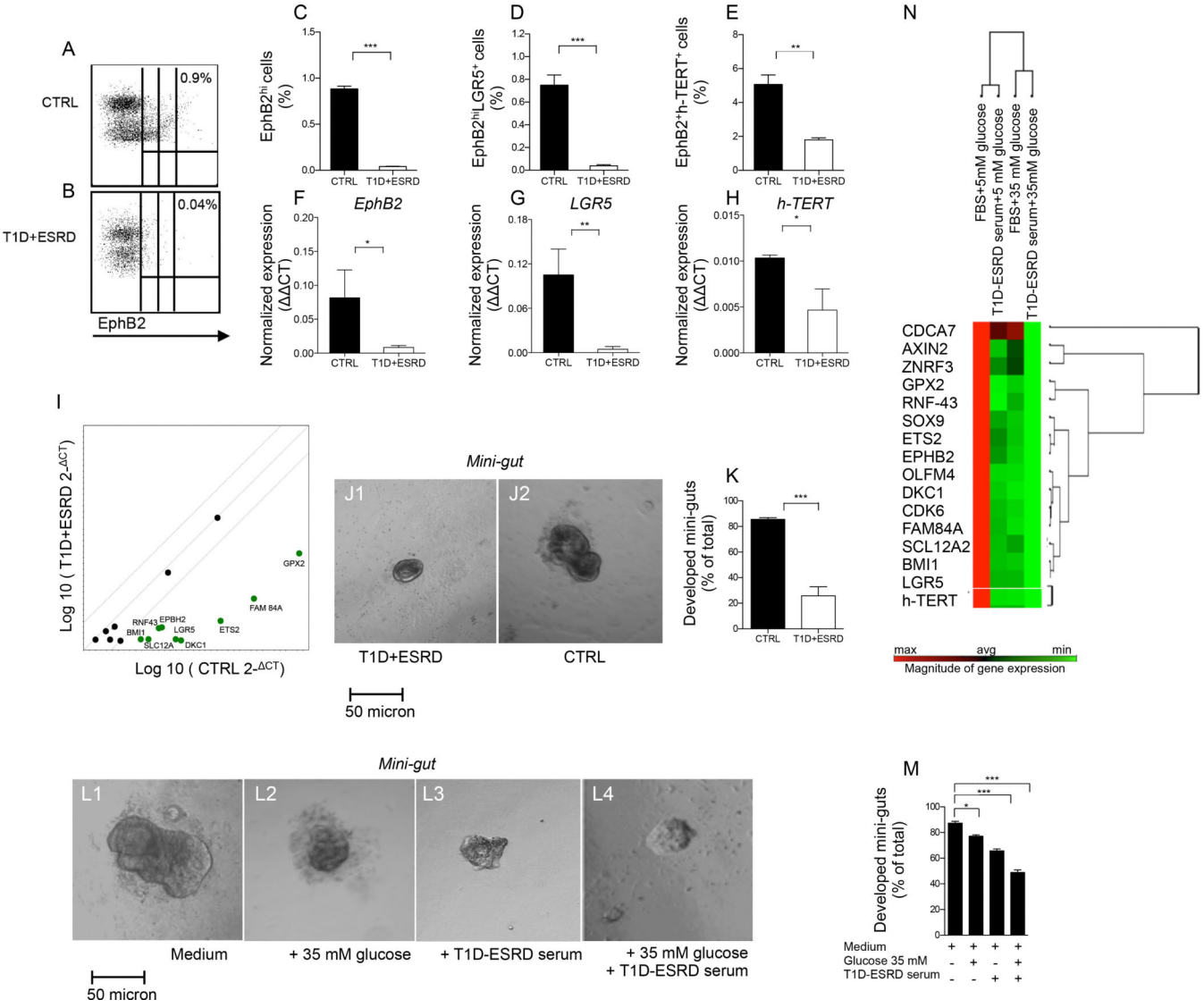

Figure 2. Diabetic enteropathy in long-standing T1D is associated with a defect in CoSCs

A, B. Representative flow dot plots of EphB2^{low}, EphB2^{medium} and EphB2^{hi} cells in healthy subjects (CTRL) and long-standing T1D individuals (T1D+ESRD). **C, D, E**. Bar graphs depict results of flow cytometric analysis of EphB2^{hi+}, EphB2^{hi+}LGR5^{+} and EphB2^{+}h-TERT^{+} cells in freshly isolated crypts (n=10 CTRL and n=10 T1D+ESRD). **F, G, H**. Bar graphs depict expression data of CoSC markers EphB2, LGR5, h-TERT as normalized mRNA expression measured by quantitative RT-PCR on isolated intestinal crypts. All samples were run in triplicate and normalized to expression of the housekeeping gene ACTB (ΔΔCt). **I**. Scatter plot represents the CoSC signature markers and stem cell transcriptome profiling examined in freshly isolated intestinal crypts of n=10 healthy subjects (CTRL) and n=10 long-standing T1D individuals (T1D+ESRD). **J1-J2**. Representative images of mini-guts cultured for 8 days *in vitro* obtained from previously isolated crypts of long-standing T1D individuals (T1D+ESRD) and healthy subjects (CTRL). 10X magnification. Scale bar 50 micron. **K**. Bar graph depicts the % of developed mini-guts of the total at 8 days of

culture of freshly isolated intestinal crypts from n=10 CTRL and n=10 T1D+ESRD individuals. **L1-L4**. Representative images of mini-guts obtained from previously isolated crypts of healthy subjects (CTRL) and cultured for 8 days in the following conditions: L1=normal (FBS) serum+normal glucose (5 mM); L2=T1D+ESRD serum+normal glucose; L3=normal serum+high glucose (35 mM); L4=T1D+ESRD serum+high glucose. 10X magnification. Scale bar 50 micron. **M**. Bar graph grouping % of developed mini-guts of the total at 8 days of culture from freshly isolated intestinal crypts cultured with the following conditions: normal (FBS) serum+normal glucose (5 mM); T1D+ESRD serum+normal glucose; normal serum+high glucose (35 mM); T1D+ESRD serum+high glucose. Statistical significance has been calculated within each group (normal glucose+normal serum, medium +high glucose, medium+long-standing T1D serum, high glucose+long-standing T1D serum) by comparing different culturing conditions. Comparison in the bar graph refers to all conditions vs. normal serum+normal glucose. **N**. Transcriptome profiling depicting CoSC signature markers expression in isolated crypts obtained from healthy subjects and cultured with/without high glucose and/or long-standing T1D serum. n=10 subjects per group were evaluated. Data are expressed as mean ± standard error of the mean (SEM) unless differently reported. *p<0.01; **p<0.001; ***p<0.0001. See also Figure S1.

Abbreviations: CoSC, colonic stem cell; T1D, type 1 diabetes; ESRD, end stage renal disease; CTRL, healthy subjects; EphB2, Ephrin B receptor 2; LGR5, leucine-rich repeat containing G protein-coupled receptor 5; RT-PCR, real-time polymerase chain reaction; ACTB, beta actin; FBS, fetal bovine serum.

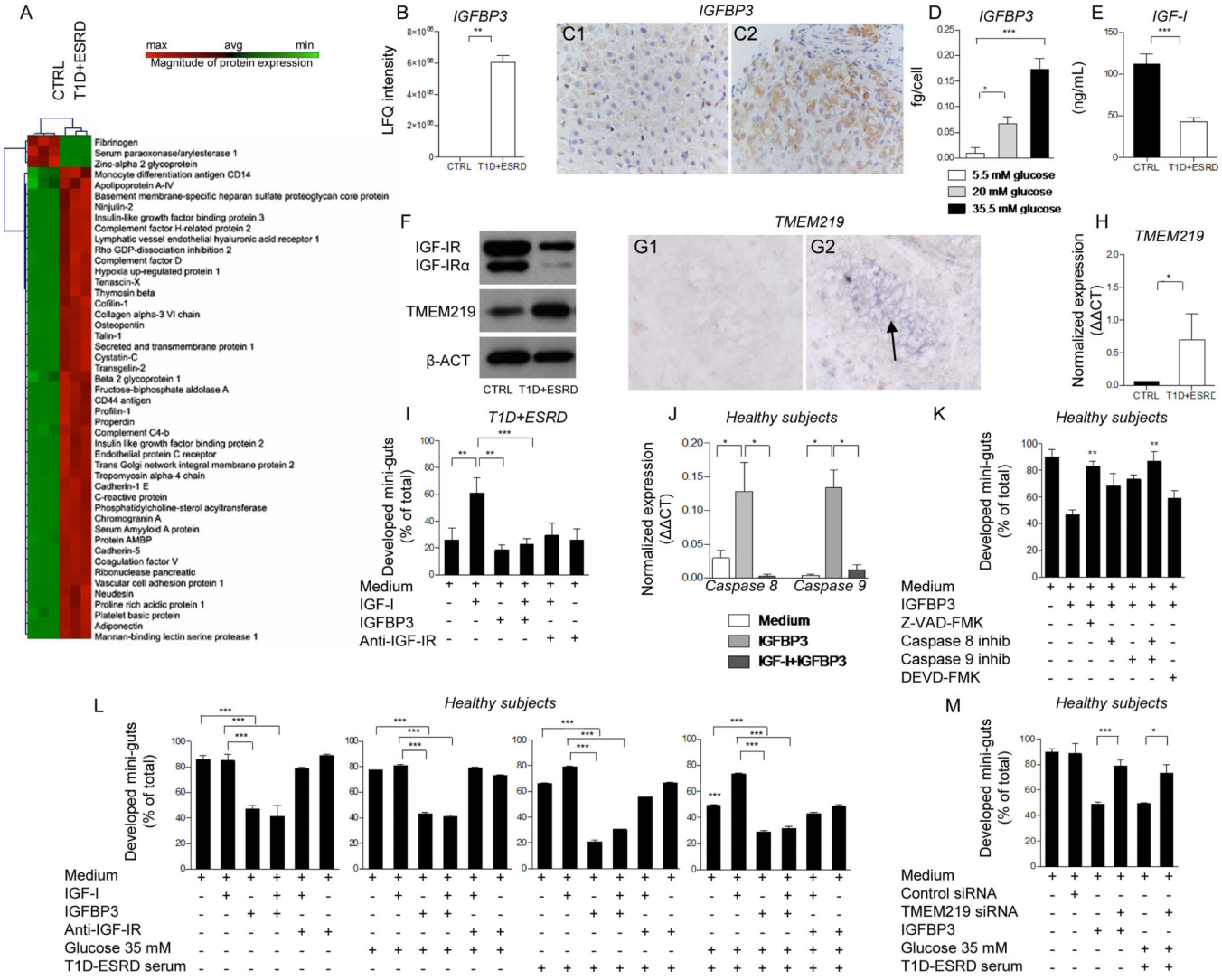

Figure 3. Circulating IGF-I and IGFBP3 are altered in long-standing T1D and its manipulation *in vitro* induces profound effects on CoSCs growth and self-renewal

A. Heat map represents the proteomic profile in long-standing T1D (T1D+ESRD) as compared to healthy subjects (CTRL). The complete dataset of identified and quantified proteins was subjected to statistical analysis ($p<0.01$). Significantly differentially expressed proteins were further analyzed through hierarchical clustering. Sera of n=10 CTRL and n=10 T1D+ESRD individuals were analyzed. **B**. Bar graph depicts LFQ intensity for a single protein extrapolated from the untargeted proteomic analysis, insulin-like growth factor binding protein 3 (IGFBP3). **C1-C2**. Representative images (40X magnification) of IGFBP3 expression in the liver. IGFBP3 is mildly and diffusely expressed in the liver parenchyma from healthy subjects (C1), while it is more zonally positive in long-standing diabetic individuals (C2). **D**. Bar graph represents IGFBP3 levels measured by ELISA in the supernatants of immortalized human hepatoma cell line (HuH-7) cultured for 5 days at different glucose concentrations (35 mM: high glucose; 20 mM: intermediate glucose; 5 mM: normal glucose). Experiments were performed in triplicate. **E**. Bar graph represents insulin-like growth factor 1 (IGF-I) levels measured by ELISA in serum of healthy subjects

and long-standing T1D (T1D+ESRD). **F**. Western blot analysis (cropped blots) confirmed IGF-IR and TMEM219 expression on the intestinal crypt surface. Evaluation of total IGF-IR expression by WB includes the detection of IGF-IRα, a subunit of IGF-IR whole protein.**G1-G2**. Representative pictures of TMEM219 in situ hybridization (G1 negative control, G2 TMEM219 staining) performed on rectal mucosa biopsy samples obtained from CTRL. 20X magnification. **H**. Bar graph depicts normalized mRNA expression of TMEM219 (IGFBP3 receptor) using the ΔΔCt method. n=5 subjects per group were evaluated. **I**. Bar graph grouping % of developed mini-guts of the total obtained from long-standing T1D individuals in different conditions and showing the effect of IGF-I, IGFBP3 and anti-IGF-IR. The p values are relative to baseline conditions and addition of IGF-I to culture. **J**. Bar graph representing normalized mRNA expression of Caspase 8 and 9 in crypts isolated from healthy subjects cultured in the presence of IGFBP3 and IGF-I +IGFBP3, performed in triplicate. **K**. Bar graph grouping % of developed mini-guts of the total at 8 days of culture, obtained from healthy subjects and cultured in the presence of a Pan-Caspase inhibitor, selective inhibitors of Caspases 8, 9 and 3, and IGFBP3. Assay was performed in triplicate. **L**. Bar graphs grouping % of developed mini-guts of the total obtained from healthy subjects and cultured in different conditions (normal glucose+normal serum, high glucose+normal serum, T1D+ESRD serum+normal glucose, T1D+ESRD serum +high glucose) and showing the effect of IGF-I, IGFBP3 and anti-IGF-IR. The p values are relative to baseline condition (medium alone, medium+high glucose, medium+long-standing T1D serum, high glucose+long-standing T1D serum). Additional p values have been calculated to compare the difference in mini-gut growth among the following conditions: medium alone vs. medium+high glucose, vs. medium+high glucose+long-standing T1D serum). Assay was performed in triplicate. **M**. Bar graph grouping % of developed mini-guts of the total obtained from healthy subjects, cultured for 8 days, exposed to TMEM219 targeting with siRNA and finally compared to TMEM219-expressing crypts in medium alone and in medium+high glucose+long-standing T1D serum. Assay was performed in triplicate. Data are expressed as mean ± standard error of the mean (SEM) unless differently reported. *p<0.01; **p<0.001; ***p<0.0001. See also Figure S1 and S2.

Abbreviations: IGF-I, insulin-like growth factor 1; IGFBP3, insulin-like growth factor binding protein 3; IGF-IR, insulin-like growth factor 1 receptor; CoSC, colonic stem cell; T1D, type 1 diabetes; ESRD, end stage renal disease; CTRL, healthy subjects; RT-PCR, real-time polymerase chain reaction; ACTB, beta actin; LFQ, Label-free quantitation; SEM, standard error of the mean; siRNA, small RNA interference; inhib, inhibitor.

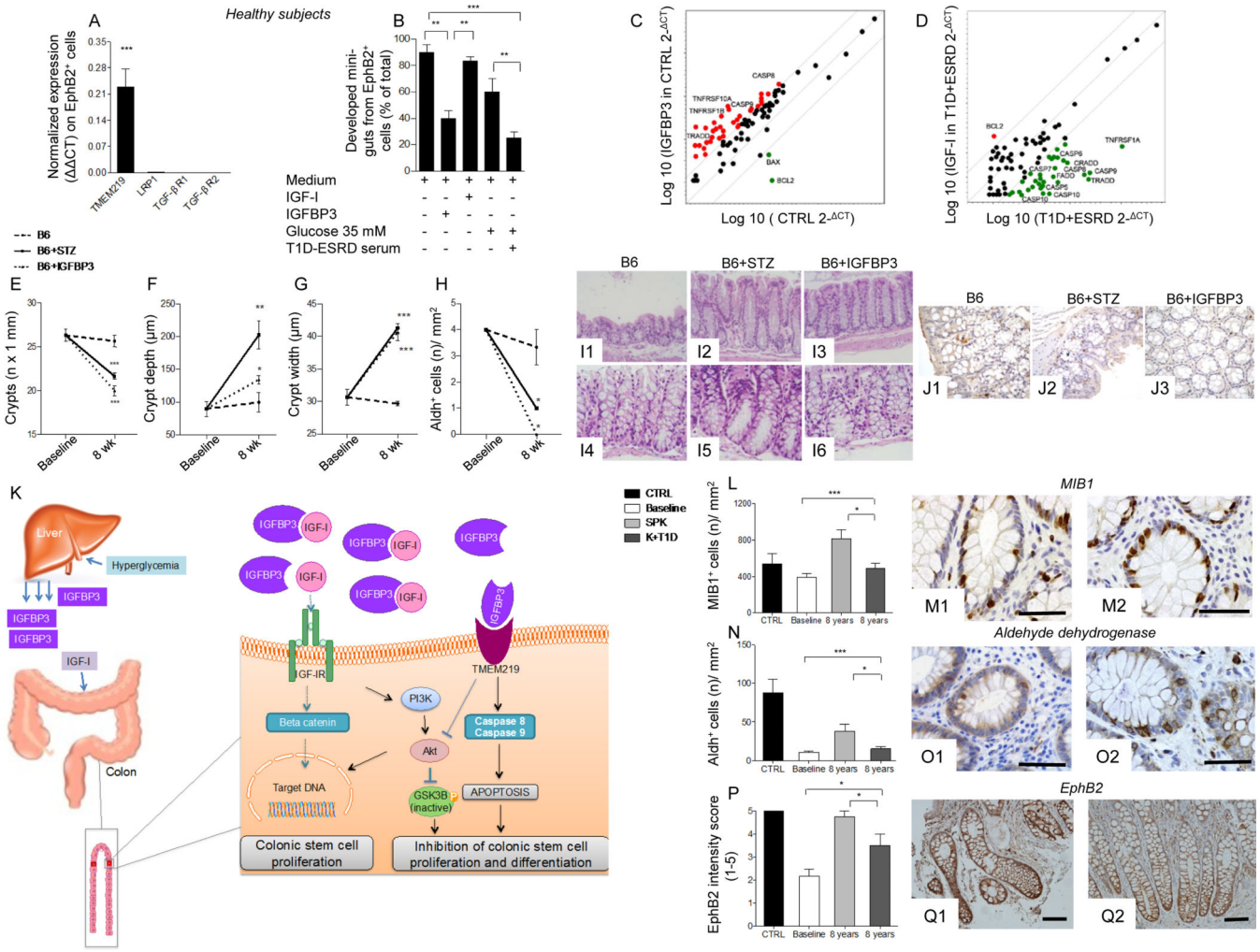

Figure 4. Effects of the peripheral IGF-I/IGFBP3 dyad on single-cell derived *in vitro* mini-guts and on caspase cascade. Manipulating the peripheral IGF-I/IGFBP3 dyad alters the progression of diabetic enteropathy in a preclinical model of diabetic enteropathy, while the treatment of long-standing T1D with simultaneous pancreas-kidney transplantation (SPK) ameliorates intestinal symptoms, motility and morphology

A. Bar graph representing normalized mRNA expression of TMEM219, LRP1, TGF-β type I and II, in EphB2^{+} sorted single cells obtained from crypts of healthy subjects. Experiments were performed in triplicate. **B**. Bar graphs showing % of developed single cell-derived mini-guts (of the total) obtained from EphB2^{+} cells sorted from freshly isolated crypts of healthy subjects and cultured in different conditions (normal glucose+normal serum, high glucose+normal serum, T1D+ESRD serum+normal glucose, T1D+ESRD serum+high glucose) and showing the effect of IGF-I and IGFBP3. The p values are relative to baseline conditions. **C**, **D**. Scatter plot representing the apoptosis transcriptome profiling examined in freshly isolated intestinal crypts of healthy subjects (CTRL) and long-standing T1D individuals (T1D+ESRD) cultured with/without IGFBP3 and IGF-I. Experiments were performed in triplicate. **E**, **F**, **G**. Line graphs reporting the number of crypts (E), depth of crypts (F) and width of crypts (G) assessed on intestinal lower tract sections harvested at baseline and after 8 weeks from STZ-treated B6 mice developing diabetic enteropathy

(B6+STZ), naïve B6 (B6), and naïve B6 treated with IGFBP3 (B6+IGFBP3). STZ: streptozoticin-treated. n=3 mice per group were evaluated. **H**. Bar graph representing the number of $Aldh^+$ cells/mm^2 in immunostained sections of STZ-treated B6 mice developing diabetic enteropathy, B6, and naïve B6 treated with IGFBP3 (B6+IGFBP3). **I1-I6**.Representative images of intestinal crypts on H&E sections of B6, B6+STZ mice developing diabetic enteropathy, and naïve B6 treated with IGFBP3 (B6+IGFBP3). Histology magnification, 200X I1-I3, 400X I4-I6. **J1-J3**. Representative images of $Aldh^+$ cells on immunostained sections of intestinal lower tract harvested from STZ-treated B6 mice developing diabetic enteropathy, B6, and naïve B6 treated with IGFBP3 (B6+IGFBP3). Histology magnification, 400X. **K**. Schematic attempt to represent the effect of circulating IGF-I and IGFBP3 on CoSCs. **L, N, P**.Bar graphs report the measurement of $MIB1^+$ and $Aldh^+$ cells, and $EphB2^+$ expression (intensity score 0-5) in the four groups of subjects (n=20 CTRL, n=30 SPK, n=K+T1D and n=60 T1D+ESRD). **M1-M2, O1-O2, Q1-Q2**. Representative images of $MIB1^+$ and $Aldh^+$ cells, and $EphB2^+$ expression in immunostained rectal mucosa bioptic samples of T1D+ESRD who underwent kidney alone (K+T1D) or simultaneous pancreas-kidney (SPK) transplantation at 8 years of follow-up. Histology magnification, 400X in M1-M2 and O1-O2, 20X in Q1-Q2. Scale bar 80 micron. Data are expressed as mean ± standard error of the mean (SEM) unless differently reported. *p<0.01; **p<0.001; ***p<0.0001. See also Figure S3, S4 and S5.

Abbreviations: STZ, streptozoticin-treated; B6, C57BL/6J mice; IGF-I, insulin-like growth factor 1; IGFBP3, insulin-like growth factor binding protein 3; IGF-IR, insulin-like growth factor 1 receptor; CoSC, colonic stem cell; T1D, type 1 diabetes; ESRD, end stage renal disease; CTRL, healthy subjects; SPK, simultaneous kidney-pancreas transplantation; K+T1D, kidney transplantation alone in type 1 diabetes; H&E, hematoxylin and eosin; MIB1, antibody against Ki67; EphB2, Ephrin B receptor 2; Aldh, Aldehyde dehydrogenase; SEM, standard error of the mean.

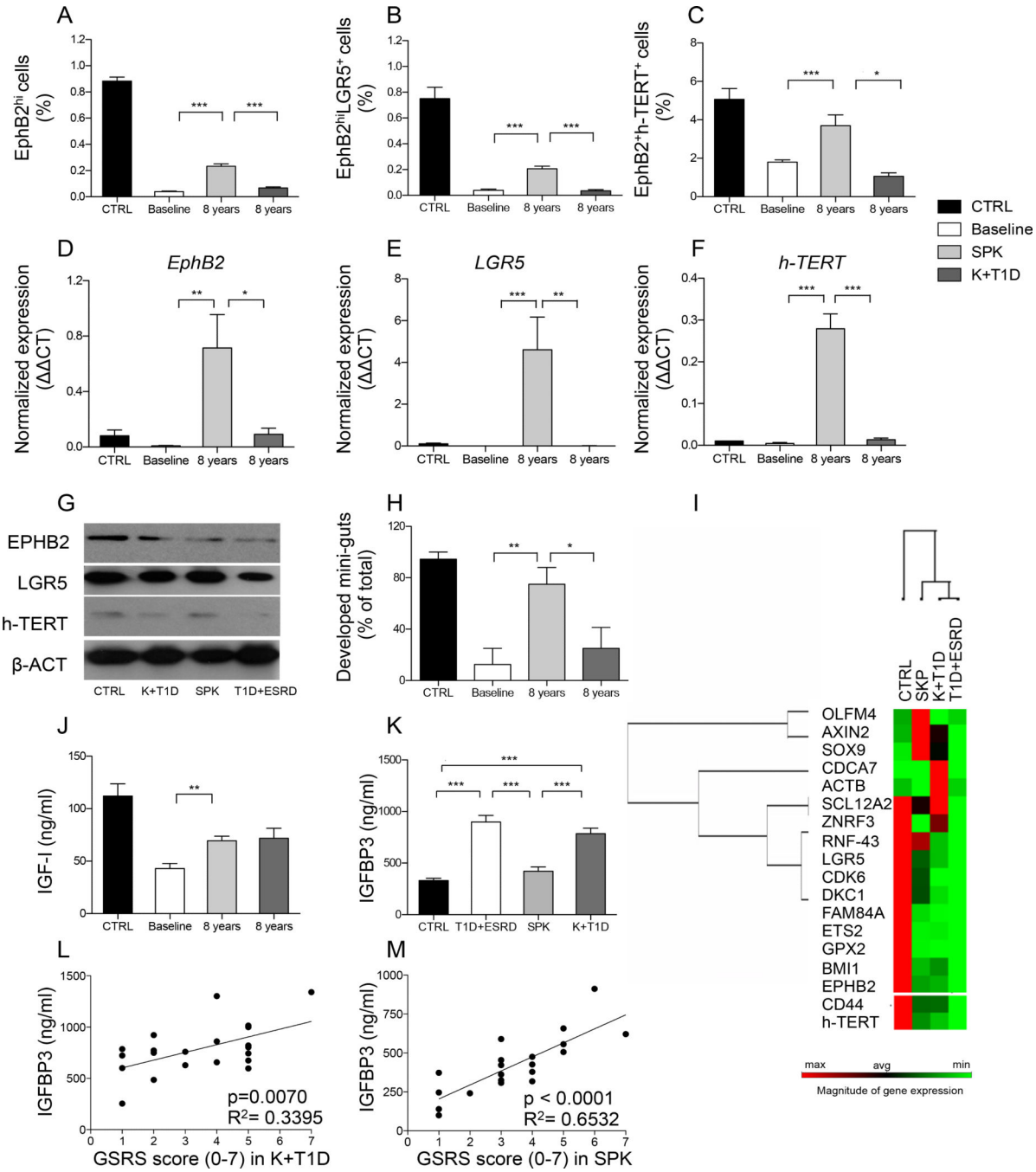

Figure 5. Treatment of long-standing T1D with SPK replenishes CoSCs and restores the CoSC signature profile and mini-gut development through restoration of circulating IGF-I and IGFBP3

A, B, C. Bar graphs depict results of flow cytometric analysis of EphB2^{hi+}, EphB2^{hi+}LGR5^{+}, EphB2^{+}h-TERT^{+} cells obtained from isolated crypts in long-standing T1D (Baseline), T1D+ESRD who underwent kidney pancreas (SPK) or kidney alone (K+T1D) transplantation at 8 years of follow-up. n=10 subjects per group were evaluated. **D, E, F**. Bar graphs depict normalized mRNA expression of intestinal stem cell markers EphB2, LGR5, h-TERT, measured by quantitative RT-PCR on isolated intestinal crypts obtained from long-

standing T1D (Baseline), T1D+ESRD who underwent kidney pancreas (SPK) or kidney alone (K+T1D) transplantation at 8 years of follow-up. All samples were run in triplicate and normalized to expression of the housekeeping gene ACTB using the ΔΔCt method. n=10 subjects per group were evaluated. **G**. Western blot analysis depicts the expression of EphB2, LGR5, h-TERT in isolated intestinal crypts of the four groups at 8 years of follow-up. n=5 subjects per group were evaluated. **H**. Bar graph depicts the % of developed mini-guts of the total at 8 days of culture of freshly isolated intestinal crypts obtained from long-standing T1D individuals (Baseline), SPK and K+T1D subjects at 8 years of follow-up. n=10 subjects per group were evaluated. **I**. Heat map represents the CoSC signature marker transcriptomic profiling examined in freshly isolated intestinal crypts of CTRL, long-standing T1D individuals (T1D+ESRD), SPK and K+T1D subjects at 8 years of follow-up. n=10 subjects per group were evaluated. **J**. Bar graph represents IGF-I levels measured by ELISA in serum of the four groups of subjects at 8 years of follow-up. n=10 subjects per group were evaluated. **K**. Bar graph depicts IGFBP3 levels measured by ELISA in serum of the four groups of subjects. n=20 subjects per group were evaluated. **L**, **M** Correlation between IGFBP3 serum levels and intestinal symptoms assessed using the GSRS questionnaire (0-7) in n=20 subjects of K+T1D (L) and SPK (M) group. Analysis was conducted using ANOVA ($p<0.05$) in comparing all groups. Data are expressed as mean ± standard error of the mean (SEM) unless differently reported. *$p<0.01$; **$p<0.001$; ***$p<0.0001$. See also Figure S5 and S6.

Abbreviations: CoSC, colonic stem cell; T1D, type 1 diabetes; ESRD, end stage renal disease; CTRL, healthy subjects; SPK, simultaneous kidney-pancreas transplantation; EphB2, Ephrin B receptor 2; LGR5, leucine-rich repeat containing G protein-coupled receptor 5; RT-PCR, real-time polymerase chain reaction; ACTB, beta actin; K+T1D, kidney transplantation alone in type 1 diabetes; IGF-I, insulin-like growth factor 1; IGFBP3, insulin-like growth factor binding protein 3; SEM, standard error of the mean.

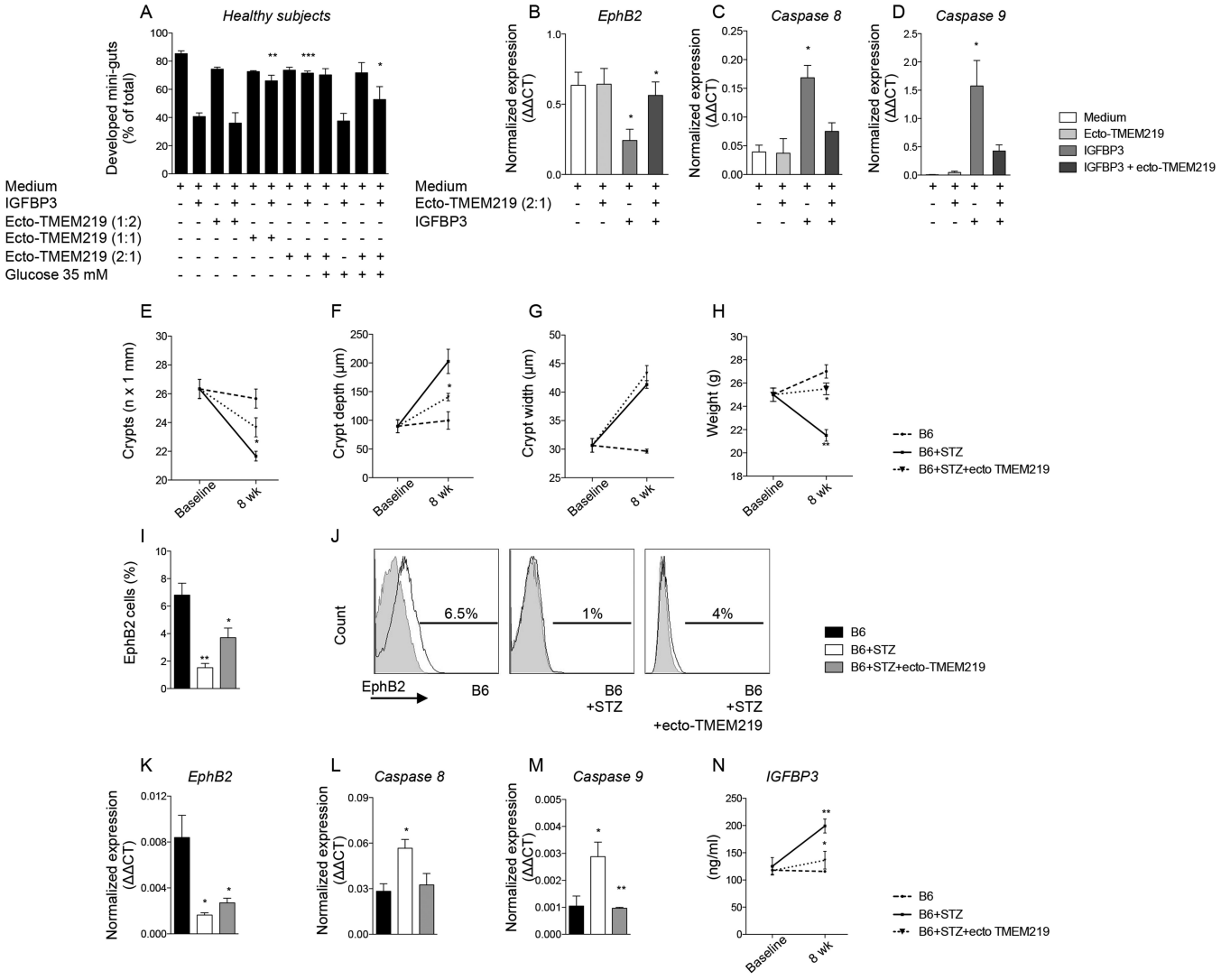

Figure 6. Treatment with the newly generated recombinant protein ecto-TMEM219 (ecto-TMEM219) abrogates IGFBP3-mediated mini-gut destruction and preserves CoSCs in a preclinical model

A. Bar graph grouping % of developed mini-guts of the total obtained from healthy subjects in different conditions and showing the effect of ecto-TMEM219 at various concentrations (1:2, 1:1 and 2:1 molar ratio as compared to IGFBP3) in IGFBP3-treated mini-guts and in those exposed to high glucose. The p values are relative to baseline conditions. **B**. Bar graph representing normalized mRNA expression of EphB2 in crypts isolated from healthy subjects cultured in the presence of IGFBP3 and ecto-TMEM219+IGFBP3, performed in triplicate. **C**, **D**. Bar graphs representing normalized mRNA expression of Caspases 8 and 9 in crypts isolated from healthy subjects cultured in the presence of IGFBP3 and ecto-TMEM219+IGFBP3, performed in triplicate. **E, F, G**. Line graphs reporting the number of crypts (E), depth of crypts (F) and width of crypts (G) assessed on intestinal lower tract sections harvested at baseline and after 8 weeks from STZ-treated B6 mice developing diabetic enteropathy (B6+STZ), naïve B6 (B6), and STZB6 mice treated with ecto-TMEM219. STZ: streptozoticin-treated. n=3 mice per group were evaluated. **H**. Line graph

reporting the weight at baseline and after 8 weeks of STZ-treated B6 mice developing diabetic enteropathy (B6+STZ), naïve B6 (B6), and of STZ-treated B6 mice developing diabetic enteropathy treated with ecto-TMEM219. STZ: streptozoticin-treated. n=3 mice per group were evaluated. **I**. Bar graph representing results of flow cytometric analysis of $EphB2^+$ cells isolated from intestinal samples collected from naïve B6 mice, STZ-treated B6 mice and in STZ-B6 mice treated with ecto-TMEM219 at 8 weeks. **J**. Representative flow histograms of $EphB2^+$ cells isolated from crypts isolated from naïve B6 mice, STZ-treated B6 mice and in STZ-B6 mice treated with ecto-TMEM219 at 8 weeks. n=3 to 5 mice per group were evaluated. **K**. Bar graph representing normalized mRNA expression of EphB2 in intestinal samples collected from naïve B6 mice, STZ-treated B6 mice and in STZ-B6 mice treated with ecto-TMEM219 at 8 weeks. **L, M**. Bar graph representing normalized mRNA expression of Caspase 8 (L) and Caspase 9 (M) in intestinal samples collected from naïve B6 mice, STZ-treated B6 mice and in STZ-B6 mice treated with ecto-TMEM219 at 8 weeks. **N**. Line graph representing murine IGFBP3 circulating levels measured in naïve B6 mice (B6) and STZ-treated B6 mice (B6+STZ) and in B6+STZ mice treated with ecto-TMEM219 at baseline and after 8 weeks. n=3 to 5 mice per group. Data are expressed as mean ± standard error of the mean (SEM) unless differently reported. *p<0.01; **p<0.001; ***p<0.0001. See also Figure S6.

Abbreviations: STZ, streptozoticin-treated; B6, C57BL/6J mice; IGF-I, insulin-like growth factor 1; IGFBP3, insulin-like growth factor binding protein 3; CoSC, colonic stem cell; H&E, hematoxylin and eosin; EphB2, Ephrin B receptor 2; SEM, standard error of the mean, T1D, type 1 diabetes; ESRD, end stage renal disease; CTRL, healthy subjects; RT-PCR, real-time polymerase chain reaction; ACTB, beta actin.